HHS Public Access

Author manuscript

Clin Cancer Res. Author manuscript; available in PMC 2020 April 01.

Published in final edited form as:

Clin Cancer Res. 2019 April 01; 25(7): 2136–2143. doi:10.1158/1078-0432.CCR-18-2684.

Elastography can map the local inverse relationship between shear modulus and drug delivery within the pancreatic ductal adenocarcinoma microenvironment

Hexuan Wang[1], **Reem Mislati**[1], **Rifat Ahmed**[1], **Phuong Vincent**[2], **Solumtochukwu Nwabunwanne**[1], **Jason R. Gunn**[2], **Brian W. Pogue**[2], and **Marvin M. Doyley**[1]

[1]University of Rochester, Department of Electrical & Computer Engineering, Rochester, NY, USA

[2]Thayer School of Engineering, Dartmouth College, Hanover NH 03755

Abstract

Purpose: High tissue pressure prevents chemotherapeutics from reaching the core of pancreatic tumors. Therefore, targeted therapies have been developed to reduce this pressure. While point probes have shown the effectiveness of these pressure-reducing therapies via single location estimates, ultrasound elastography is now widely available as an imaging technique to provide real-time spatial maps of shear modulus (tissue stiffness). However, the relationship between shear modulus and the underlying tumor microenvironmental causes has not been investigated. In this work, elastography was used to investigate how shear modulus influences drug delivery *in situ*, and how it correlates with collagen density, hyaluronic acid content, and patent vessel density, features of the tumor microenvironment known to influence tissue pressure.

Experimental Design: Intravenous injection of verteporfin, an approved human fluorescent drug, was used in two pancreatic cancer xenograft models (AsPC1 (n=25) and BxPC3 (n=25)).

Results: Fluorescence intensity was higher in AsPC-1 tumors than in BxPC-3 tumors ($p < 0.0001$). Comparing drug uptake images and shear wave elastographic images with histological images revealed that: (1) drug delivery and shear modulus were inversely related, (2) shear modulus increased linearly with increasing collagen density, and (3) shear modulus was marginally correlated with the local assessment of hyaluronic acid content.

Conclusions: These results demonstrate that elastography could guide targeted therapy and/or identify patients with highly elevated tissue pressure.

Keywords

Shear modulus; pancreatic ductal adenocarcinoma; elastography; tumor microenvironment; targeted therapies

Corresponding author: Marvin M. Doyley, PhD, University of Rochester, 723 Computer Studies Building, Box 270231, Rochester, NY 14627-0126, Tel: +1 (585) 275-3774, Fax: +1 (585) 275-2073, m.doyley@rochester.edu.

Conflict of interest: The authors declare no potential conflicts of interest.

Introduction

High tissue pressures prevent effective treatment of pancreatic ductal adenocarcinoma (PDA), the most common form of pancreatic cancer, which is a lethal disease with a 5-year survival rate of less than 7 % (1). Currently, surgical resection is the most effective treatment, but only 20% of patients have a resectable tumor at diagnosis (2,3). For patients with borderline resectable tumors, neoadjuvant chemotherapy can sometimes enable downstaging of disease for surgical resection (4,5), but high tissue pressures (on the order of 10–100 mmHg) can prevent chemotherapeutic agents from reaching the tumor core (6–8). Leaky vasculature, high stromal density, and high hyaluronic acid content all increase tissue pressure heterogeneously (9–12). Consequently, several groups are now developing targeted therapies to reduce pressure. These therapies include the ablation of hyaluronic acid with PEGPH20 (6,13–15), losartan (16–18), and stromal targeting (19–21). PEGPH20 in combination with Gemcitabine is currently undergoing Phase I/II clinical trials. Early results indicate that patients with metastatic PDA suffered no adverse reaction when PEGPH20 was administered in combination with Gemcitabine (15,22). However, choosing the most appropriate pressure-reducing therapies is difficult because no technique can measure tissue pressure *in vivo*.

Researchers have used invasive pressure catheters (23) to evaluate the effectiveness of different pressure-reducing therapies either with animal models or, to a lesser extent, in the clinic. Current catheters measure tissue pressure by using either the piezoelectric effect or the wick-in-needle method. Piezoelectric catheters measure the stress (solid stress and interstitial fluid pressure) exerted on the active element at the probe's insertion point, while catheters based on the wick-in-needle method measure the interstitial fluid pressure transmitted through saline solution within the catheter. Provenzano and colleagues (6,24) used a piezoelectric catheter to measure the interstitial fluid pressure within murine pancreatic tumors and to demonstrate that depleting the tumor microenvironment of hyaluronic acid reduces interstitial fluid pressure. Researchers have also used a wick-in-needle pressure catheter to predict the outcome of patients with cervical cancer (25). Despite these important preclinical and clinical results, the invasive nature of pressure catheters and their inability to measure the spatial variation of tissue pressure (23,26) have limited their clinical use. Elastography could overcome these limitations by providing a surrogate measure to tissue pressure.

Elastography uses a three-step process to visualizes shear modulus, an intrinsic property of soft tissues that is defined as the ratio of shear stress to shear strain. First, motion is induced within the tissue using either an external or internal mechanical stimulation. Second, ultrasound measures the spatial variation of the mechanical response. Third, shear modulus is inferred by applying either a simplified or continuum mechanical model to the measured mechanical response (27). Although elastography cannot measure tissue pressure directly, the steep pressure gradient at the tumor margin exerts mechanical stress on the extracellular matrix (ECM) and the stromal cells, which in turn increases shear modulus (28). Our long-term goal is to establish that shear modulus distribution measured non-invasively and in real-time with elastography is a good alternative to tissue pressure measurements.

The goal of this work was to use elastography, mapping point by point within spatially-registered images, to assess (a) the relationship between shear modulus and drug delivery in PDA, and (b) the relationship between shear modulus and patent vessel density, hyaluronic acid content, and collagen density. To achieve these goals, we used mice bearing two very different phenotypic PDA tumor models, AsPC-1 (n=25) and BxPC-3 (n=25), imaging drug uptake from verteporfin, a fluorescent drug FDA-approved for human use, and then mapping the same tumors for shear modulus. AsPC-1 tumors grow much faster and have higher chemotherapy drug uptake (29) than their BxPC-3 counterparts. Both groups of tumors were both derived from human PDA. Specifically, we obtained BxPC-3 cells from the primary tumor and AsPC-1 cells from ascites of a metastatic site.

Materials and Methods

This section describes the tumor models, imaging protocols (shear wave elasticity imaging and fluorescence), and histological and statistical analysis used in this study. The Animal Care and Use Committee of the University of Rochester and Dartmouth College approved all animal protocols, and the procedures used here followed these approved protocols (#101759/2016–024).

Tumor Models

A total of 25 AsPC-1 (ATCC, Cat#CRL-1682) and 25 BxPC-3 (ATCC, Cat#CRL-1687) tumors were grown orthotopically in the pancreas of female nude mice (4 months old, 225g, Athymic nude mice Charles Rivers Laboratories, Wilmington, MA, USA). We injected 10^6 tumor cells in Matrigel™ (BD Biosciences, San Jose, California, USA) and 50% media orthotopically in the pancreas of each animal. All tumors were allowed to grow until their volume was between 100–200mm^3. AsPC-1 tumors reached the desired volume range within 4 to 6 weeks; however, BxPC-3 tumors took 10 weeks to reach the same volume (30,31).

Shear wave elasticity imaging (SWEI)

We used the single-track-location shear wave elastographic imaging (STL-SWEI) method to visualizes the shear modulus distribution of excised tumors, which we recently implemented on a Vantage 64 ultrasound scanner (Verasonics Inc., Kirkland, WA, USA) equipped with an L7–4 (Phillips Healthcare, Andover, MA, USA) linear transducer array (32). During STL-SWEI, we used ultrasound beams to both induce and track shear wave propagation in tissues. We estimated the speed of shear waves produced with a pair of laterally spaced push beams at a fixed location with a single tracking beam. To create an image, we transmit several pairs of push beams within the tissue. We then combined local tissue density (ρ) with shear wave speed (SWS) to get regional shear modulus estimates ($\mu = \rho \times SWS^2$). All tumors were surgically removed and encased in a 216mm^3 gelatin block as previously described (33) to minimize the impact of respiration and cardiac motion on shear waves estimates (see Fig. S1a–b). Each gelatin block consisted of 10% by weight porcine skin gelatin (300 bloom, Type A, Sigma-Aldrich Corporation, St. Louis, MO, USA), 1% by weight corn starch (Sigma-Aldrich Corporation, St. Louis, MO, USA), and 89% by weight high purity water (18 MΩ). All SWEI was performed using 5MHz pushing and tracking

beams. The focal lengths of both beams (pushing and tracking) were placed at the center of each tumor, which corresponded to scan depths ranging from 20–30 mm depending on the tumor volume. A 400 μs push pulse was used to induce shear waves in the gelatin-encapsulated tumors, at a pulse repetition frequency of 7 kHz. For each transmitted pulse, we acquired multiple tracking A-lines (a lateral line density of ≈4 beams/mm) from a 2 cm wide region-of-interest. For each cancer, shear wave elastographic images were acquired from multiple cross-sections (n=10)—corresponding to slice intervals of ≈ 2mm (see Fig. S2). To minimize registration errors between the shear wave and histological images, the central scan plane was marked as illustrated in Fig. S1c–f.

Fluorescence imaging

To assess how shear modulus relates to drug delivery, an FDA-proved fluorescent drug was used (1 mg/kg verteporfin, MW 719 DA; Sigma-Aldrich, St. Louis, MO, USA) for intravenous injection into each mouse via the tail vein, one hour before sacrifice (34–36). To determine the relationship between blood vessel density and drug uptake, 1 mg/kg of Lectin (Vector Laboratories, CAT# FL-1211, Burlingame, CA, USA), a fluorescence stain, was injected intravenously into all tumor-bearing mice one minute prior to sacrifice. After tissue prep and sectioning, slices of tissue were scanned on a flatbed scanner (GE Typhoon 9410, GE Healthcare, Piscataway, NJ, USA) and a PerkinElmer Vectra 3.0 fluorescence slide scanner (Waltham, MA, USA) to acquire verteporfin and Lectin fluorescence images.

Histological Analysis

To quantify collagen density, patent vessel density, and fluorescence uptake, quantitative histology was calculated from all excised tumors. All tumors were formalin-fixed and embedded in paraffin for thin sectioning (2 μm) and stained with Masson's trichrome (MT) stain, hyaluronic acid binding protein (HABP-1) (37), and Lectin, after imaging. The fluorescence slide scanner was used to image each section, and a three-step color segmentation process (see Fig. S3) was implemented in MATLAB (v2016b, The Mathworks Inc., Natick, MA, USA) to estimate collagen density from the Masson's trichrome stained images (26). Collagen density (%) was calculated by dividing the number of blue collagen pixels by the total number of pixels in the tumor. We used a similar analysis to quantify hyaluronic acid density (%).

A global thresholding algorithm was used to isolate pixels stained with Lectin fluorescence images, and so the patent vessel density (%) was estimated by dividing the number of Lectin-stained pixels by the total number of pixels in the tumor.

Verteporfin perfusion was estimated from the fluorescence maps, by defining regions of interest (ROI) within the fluorescence images and computing the mean fluorescence intensities within these.

Statistical Analysis

We used a linear regression analysis to determine the correlation between the measured biomarkers (e.g., collagen density, patient vessel density, hyaluronic acid content, drug uptake, and shear modulus). Statistical significance was determined from the differences in

measured biomarkers of each tumor type using a Welch's t-test. All statistical analysis was performed with Prism v7.0 for Mac (GraphPad, La Jolla, CA, USA).

Results

Drug uptake is lower in stiffer tumors than softer ones

To understand how shear modulus affects drug uptake, the fluorescence intensity of verteporfin was measured and compared to the mean shear modulus of the two groups of excised tumors (AsPC-1 and BxPC-3). We performed a quantitative analysis of Masson's trichrome and Lectin-stained histological images to quantify differences in collagen and patent vessel density, factors known to impact drug delivery and tissue pressure. Figure 1 shows box plots of fluorescence intensity (verteporfin uptake), shear modulus, collagen density, and patent vessel density for the two groups of tumors. Fluorescence intensity in AsPC-1 was three times higher than that measured in BxPC-3 tumors (Fig. 1(a)). The mean shear modulus of AsPC-1 tumors was 36.07 kPa lower than their counterparts (Fig. 1(b)). Univariate analysis of variance (ANOVA) revealed that this difference was significant ($p = 0.0008$; F-number= 11.87). ANOVA also revealed a within-group variance of 7.46 kPa and 7.35 kPa for AsPC-1 and BxPC-3 tumors, respectively. The observed difference in the shear modulus reflects differences in the total tissue pressure (solid stress and interstitial fluid pressure). The observed differences in shear modulus and fluorescence intensity were statistically significant ($p < 0.0001$ and $p < 0.001$). BxPC-3 tumors had higher collagen density (Fig. 1(c) and Fig. 2). AsPC-1 tumors had higher patent vessel density than their BxPC-3 counterparts (Fig. 1(d)).

Patent vessel density is linearly related to drug delivery and inverse related to shear modulus

To understand the relationship between patent vessel density to both drug uptake and shear modulus, we assessed the mean properties (shear modulus, patent vessel density, and fluorescence intensity) measured for each tumor. This analysis revealed that patent vessel density and verteporfin uptake were linearly related (Fig. 3(a)). Additionally, there was a strong inverse correlation between patent vessel density and shear modulus (Fig. 3(b)). This suggests that the high shear modulus of the extracellular matrix (ECM), which compresses tumor vasculature, is the primary mechanism that impedes drug delivery.

Shear modulus and drug delivery are inversely related

Figure 4 (a-d) shows representative shear modulus elastograms and verteporfin uptake maps obtained from AsPC-1 and BxPC-3 tumors. For both tumor groups, shear modulus was heterogeneously distributed, which is consistent with our previous reported results (33). Fluorescence intensity was also heterogeneously distributed, which suggests that drug uptake in the tumors varied spatially (Fig. 4 (c) and (d)). Localized regions of high fluorescence intensity corresponding to localized region of low shear modulus; whereas, regions with low fluorescence intensities corresponding to high shear modulus. Further analysis revealed that shear modulus and verteporfin fluorescence intensity were inversely related (Fig. 4(e)). The fluorescence intensities of AsPC-1 tumors were consistently higher

than those obtained from BxPC-3 tumors—a trend that was consistent with our previous study performed with a pressure probe (26).

Hyaluronic acid density is weakly associated with shear modulus

The pancreatic cancer tumor microenvironment often contains high levels of hyaluronic acid (HA), which increases interstitial fluid pressure (9–12,38). For both groups of tumors, HA density was lower than collagen density (Fig. 5 (b) and (c)) but was distributed heterogeneously throughout the tumors. Global assessment of HA density revealed no significant difference in HA between the two groups of tumors or any correlation between HA density and shear modulus (Fig. 5(e)). Localized assessment of the tumors (identifying areas of different HA density on the HABP1-stained images and relating these to the corresponding areas in registered shear modulus elastograms) revealed a weak correlation between HA density and shear modulus (Fig 5(f)).

Discussion

In this work, imaging of elastography and drug fluorescence within two xenograft pancreatic cancer tumor models (AsPC-1 and BxPC-3) was used to study how the shear modulus correlates with drug delivery, patent vessel density, collagen density and HA content. AsPC-1 tumors were perfused with more fluorescent verteporfin, than their BxPC-3 counterparts (Fig. 1(a)) due to differences tissue pressure that were measured indirectly using shear modulus (Fig. 1(b)). Solid stress and interstitial fluid pressure both influence tissue pressure; therefore, to understand which of these two sources are responsible for the observed difference in shear modulus, we measured collagen density and hyaluronic acid content of all tumors. The BxPC-3 tumors had higher collagen density than AsPC-1, but their hyaluronic acid content was similar. Stiffer tumors were more collagen-rich than softer ones (Fig. 2). Drug uptake increased linearly with patent vessel density (Fig. 3) but decreased linearly with increasing shear modulus (Fig. 3). Patent vessel density was inversely related to shear modulus, suggesting that increasing total tissue pressure may cause vessels to collapse and impede drug delivery (Fig. 5).

Clinical trends predict that pancreatic cancer will be the second leading cause of all cancer-related deaths in the United States (39). Consequently, developing therapies for either treating the disease or allowing more patients to qualify for surgery is an area of active research (4,5). High tissue pressure can impede the delivery of therapeutic agents and encourage tumor progression (40,41). Tissue pressure is difficult to measure with current invasive pressure catheter. No imaging technique can measure tissue pressure *in vivo* today, but we have previously demonstrated that shear modulus is a good surrogate. Using a modified invasive pressure catheter, it was shown that drug delivery in both AsPC-1 and BxPC-3 were inversely related to pressure, which is consistent with Fig. 3. Our current work is the first demonstration that shear modulus imaging correlates with drug uptake. Specifically, drug delivery is inversely related to shear modulus, and hence tissue pressure. This implies that imaging could be used to evaluate how well a given therapy reduces shear modulus, and this information could serve as a surrogate for drug penetration.

Preclinical studies demonstrate that depleting the tumor microenvironment of HA lowers interstitial fluid pressure, restores vasculature, and improves permeability to chemotherapeutics (42,43). Figure 5(a) demonstrates that globally there is no correlation between HA and shear modulus. This would imply that SWEI could prove to be an ineffective method for monitoring the efficacy of HA ablation. Although consistent with the results reported by (44), it contradicts our previous results that showed that shear modulus correlated with HA content. The discrepancy in the current results and our previous results is shown in Fig. 5(e) and is due to differences in the analysis in the two reports. Specifically, in (33), local analysis of HA and shear modulus was performed, whereas in our current work the analysis was performed globally. HA concentrates in localized regions within many cancerous tissues. Thus, when HA absorbs water and swells, it exerts pressure on the collagen-rich extracellular matrix that produces an equal but opposing force in the localized region. The magnitude of the resulting pressure depends on the amount of water absorbed and the shear modulus of the ECM (i.e., the higher the shear modulus, the higher the localized pressure) as we have previously demonstrated (33). We expect the global stiffness of the ECM will increase when the number of HA pockets exceeds a critical value or when the localized HA pockets are located in areas of abnormally high collagen density. We observed neither of these phenomena when HABP-1 stain histological slides were analyzed; therefore, the observation that global estimates of shear modulus and HA density (Fig 5e) were not related. Figure 5(f) revealed a weak but significant correlation between the local estimates of HA and shear modulus. However, because of differences in the frequency of the transducers used (10 MHz vs. 5 MHz), there was higher variability in measured shear modulus. Therefore, higher frequency probes and methods such as plane-wave-single-track location elastography (32) should prove more useful in monitoring HA ablation with shear modulus.

Several groups have proposed the use of radiotherapy (45–47), anti-stromal therapy (19–21), and targeting hyaluronic acid (6,13,14) to reduce tissue pressure. Stromal density is responsible for high tissue pressure; therefore, we predict that anti-stromal therapy will yield the greatest reduction in tissue pressure. We are currently conducting preclinical studies to corroborate this expectation. If this proves to be true, this would allow clinical researchers to assess the efficacy of anti-stromal therapy without relying on endpoint studies.

The current study has three main limitations. First, all studies were performed with immunocompromised animals, therefore it is not clear how the immune system will impact the results. Preclinical studies demonstrated that targeting the CCR2/CCR5 chemokines axes improves immune response and the efficacy of radiotherapy (48). Irradiated mouse tumors are palpably softer than non-irradiated tumors, which suggests that besides increasing immune response, combining radiotherapy with CCR2 targeting also reduces total tissue pressure in PDA. Second, all analysis was performed on excised samples; therefore, we could not study how survival correlates with shear modulus. However, this methodology was used in order to obtain highly registered images with histology. Advanced SWEI techniques could be used *in vivo* for assessment of shear modulus in future studies. Third, no control group was included in this study. AsPC-1 and BxPC-3 tumors uptake different amounts of fluorescence which suggests that there are surrogate reporters for vascular perfusion, and hence chemotherapy uptake. Higher fluorescence uptake is known to correlate with higher

vascular delivery of systemic agents. Thus, the two tumors present cases for lower and higher chemotherapy uptake (29).

In this paper, two xenograft models (AsPC-1 and BxPC-3 with different growth rates) were used to show that shear modulus directly influences drug delivery for tumors (known to have higher (AsPC-1) and lower (BxPC-3) chemotherapy uptake) and that the pathologically-measured tumor microenvironment modulates the shear modulus. Although local and global estimates of tumor stiffness are dependent on collagen density, this was not necessarily the case for hyaluronic acid. Specially, a strong correlation was shown between the local estimate of shear modulus and hyaluronic acid content for the two groups for tumors, but global estimation showed no such correlation. This suggests that elastography could, in principle, monitor local changes in tissue pressure during anti-stromal therapy and hyaluronic acid depletion, but monitoring HA depletion could prove more challenging since this will require local assessment whose accuracy will depend on the resolution of the resulting elastograms.

Supplementary Material

Refer to Web version on PubMed Central for supplementary material.

Acknowledgments

Financial support: This work supported by NIH grants R56EB024320 and P01CA084203

References

1. Duggan MA, Anderson WF, Altekruse S, Penberthy L, Sherman ME. The Surveillance, Epidemiology, and End Results (SEER) Program and Pathology: Toward Strengthening the Critical Relationship. Am J Surg Pathol 2016;40(12):e94–e102 doi 10.1097/PAS.0000000000000749. [PubMed: 27740970]
2. Li D, Xie K, Wolff R, Abbruzzese JL. Pancreatic cancer. Lancet 2004;363(9414):1049–57 doi 10.1016/S0140-6736(04)15841-8. [PubMed: 15051286]
3. Jemal A, Siegel R, Ward E, Hao Y, Xu J, Thun MJ. Cancer statistics, 2009. CA Cancer J Clin 2009;59(4):225–49 doi 10.3322/caac.20006. [PubMed: 19474385]
4. Katz MH, Crane CH, Varadhachary G. Management of borderline resectable pancreatic cancer. Semin Radiat Oncol 2014;24(2):105–12 doi 10.1016/j.semradonc.2013.11.006. [PubMed: 24635867]
5. Lal A, Christians K, Evans DB. Management of borderline resectable pancreatic cancer. Surg Oncol Clin N Am 2010;19(2):359–70 doi 10.1016/j.soc.2009.11.006. [PubMed: 20159519]
6. Provenzano PP, Cuevas C, Chang AE, Goel VK, Von Hoff DD, Hingorani SR. Enzymatic targeting of the stroma ablates physical barriers to treatment of pancreatic ductal adenocarcinoma. Cancer Cell 2012;21(3):418–29 doi 10.1016/j.ccr.2012.01.007. [PubMed: 22439937]
7. Neesse A, Heumann T, Gorg C, Kiessling A, Klose KJ, Gress TM, et al. Periportal cuffing in inflammatory bowel diseases: mystery of stars and stripes. Inflamm Bowel Dis 2010;16(8):1275–6 doi 10.1002/ibd.21165. [PubMed: 20027605]
8. Chu GC, Kimmelman AC, Hezel AF, DePinho RA. Stromal biology of pancreatic cancer. J Cell Biochem 2007;101(4):887–907 doi 10.1002/jcb.21209. [PubMed: 17266048]
9. Jain RK Baxter LT Mechanisms of heterogeneous distribution of monoclonal antibodies and other macromolecules in tumors: Significance of elevated interstitial pressure. 1989 7022–32 p.

10. Gutmann R, Leunig M, Feyh J, Goetz AE, Messmer K, Kastenbauer E, et al. Interstitial hypertension in head and neck tumors in patients: correlation with tumor size. Cancer research 1992;52(7):1993–5. [PubMed: 1551128]
11. Heine M, Freund B, Nielsen P, Jung C, Reimer R, Hohenberg H, et al. High Interstitial Fluid Pressure Is Associated with Low Tumour Penetration of Diagnostic Monoclonal Antibodies Applied for Molecular Imaging Purposes. PLOS ONE 2012;7(5):e36258 doi 10.1371/journal.pone.0036258. [PubMed: 22590529]
12. Stylianopoulos T, Martin JD, Chauhan VP, Jain SR, Diop-Frimpong B, Bardeesy N, et al. Causes, consequences, and remedies for growth-induced solid stress in murine and human tumors. Proc Natl Acad Sci U S A 2012;109(38):15101–8 doi 10.1073/pnas.1213353109. [PubMed: 22932871]
13. Provenzano PP, Hingorani SR. Hyaluronan, fluid pressure, and stromal resistance in pancreas cancer. Br J Cancer 2013;108(1):1–8 doi 10.1038/bjc.2012.569. [PubMed: 23299539]
14. Second-line Study of PEGPH20 and Pembro for HA High Metastatic PDAC. https://ClinicalTrials.gov/show/NCT03634332.
15. Study of Gemcitabine + PEGPH20 vs Gemcitabine Alone in Stage IV Previously Untreated Pancreatic Cancer. https://ClinicalTrials.gov/show/NCT01453153.
16. Losartan and Nivolumab in Combination With FOLFIRINOX and SBRT in Localized Pancreatic Cancer. https://ClinicalTrials.gov/show/NCT03563248.
17. Proton w/FOLFIRINOX-Losartan for Pancreatic Cancer. https://ClinicalTrials.gov/show/NCT01821729.
18. Chauhan VP, Martin JD, Liu H, Lacorre DA, Jain SR, Kozin SV, et al. Angiotensin inhibition enhances drug delivery and potentiates chemotherapy by decompressing tumour blood vessels. Nat Commun 2013;4:2516 doi 10.1038/ncomms3516. [PubMed: 24084631]
19. Stromal TARgeting for PAncreatic Cancer (STAR_PAC). https://ClinicalTrials.gov/show/NCT03307148.
20. Guo J, Xiao B, Lou Y, Yan C, Zhan L, Wang D, et al. Antitumor effects of all-trans-retinoic acid on cultured human pancreatic cancer cells. J Gastroenterol Hepatol 2006;21(2):443–8 doi 10.1111/j.1440-1746.2006.04180.x. [PubMed: 16509872]
21. Kuroda H, Tachikawa M, Uchida Y, Inoue K, Ohtsuka H, Ohtsuki S, et al. All-trans retinoic acid enhances gemcitabine cytotoxicity in human pancreatic cancer cell line AsPC-1 by up-regulating protein expression of deoxycytidine kinase. Eur J Pharm Sci 2017;103:116–21 doi 10.1016/j.ejps.2017.02.021. [PubMed: 28215943]
22. DuFort CC, DelGiorno KE, Hingorani SR. Mounting Pressure in the Microenvironment: Fluids, Solids, and Cells in Pancreatic Ductal Adenocarcinoma. Gastroenterology 2016;150(7):1545–+ doi 10.1053/j.gastro.2016.03.040. [PubMed: 27072672]
23. Chakraborty J, Langdon-Embry L, Cunanan KM, Escalon JG, Allen PJ, Lowery MA, et al. Preliminary study of tumor heterogeneity in imaging predicts two year survival in pancreatic cancer patients. Plos One 2017;12(12) doi ARTNe018802210.1371/journal.pone.0188022.
24. DelGiorno KE, Carlson MA, Osgood R, Provenzano PP, Brockenbough JS, Thompson CB, et al. Response to Chauhan et Al.: interstitial pressure and vascular collapse in pancreas cancer-fluids and solids, measurement and meaning. Cancer Cell 2014;26(1):16–7 doi 10.1016/j.ccr.2014.06.004. [PubMed: 25026210]
25. Milosevic M, Fyles A, Hedley D, Pintilie M, Levin W, Manchul L, et al. Interstitial fluid pressure predicts survival in patients with cervix cancer independent of clinical prognostic factors and tumor oxygen measurements. Cancer research 2001;61(17):6400–5. [PubMed: 11522633]
26. Nieskoski MD, Marra K, Gunn JR, Hoopes PJ, Doyley MM, Hasan T, et al. Collagen Complexity Spatially Defines Microregions of Total Tissue Pressure in Pancreatic Cancer. Scientific Reports 2017;7(1):1—12. [PubMed: 28127051]
27. Doyley MM, Parker KJ. Elastography: general principles and clincial applications. Ultrasound clinics 2014;9(1):1–11 doi 10.1016/j.cult.2013.09.006. [PubMed: 24459461]
28. Swartz MA, Lund AW. Lymphatic and interstitial flow in the tumour microenvironment: linking mechanobiology with immunity. Nat Rev Cancer 2012;12(3):210–9 doi 10.1038/nrc3186. [PubMed: 22362216]

29. Russell J, Pillarsetty N, Kramer RM, Romesser PB, Desai P, Haimovitz-Friedman A, et al. In Vitro and In Vivo Comparison of Gemcitabine and the Gemcitabine Analog 1-(2'-deoxy-2'-fluoroarabinofuranosyl) Cytosine (FAC) in Human Orthotopic and Genetically Modified Mouse Pancreatic Cancer Models. Molecular Imaging and Biology 2017;19(6):885–92 doi 10.1007/s11307-017-1078-6. [PubMed: 28349292]
30. Ma Y, Hwang RF, Logsdon CD, Ullrich SE. Dynamic mast cell-stromal cell interactions promote growth of pancreatic cancer. Cancer research 2013;73(13):3927–37 doi 10.1158/0008-5472.CAN-12-4479. [PubMed: 23633481]
31. Deer EL, Gonzlez-Hernndez J, Coursen JD, Shea JE, Ngatia J, Scaife CL, et al. Phenotype and genotype of pancreatic cancer cell lines. Pancreas 2010;39(4):425—35. [PubMed: 20418756]
32. Ahmed R, Gerber SA, McAleavey SA, Schifitto G, Doyley MM. Plane-Wave Imaging Improves Single-Track Location Shear Wave Elasticity Imaging. IEEE Transactions on Ultrasonics, Ferroelectrics, and Frequency Control 2018;65(8):1402–14 doi 10.1109/TUFFC.2018.2842468.
33. Wang H, Nieskoski MD, Marra K, Gunn JR, Trembly S, Pogue BW, et al. Elastographic Assessment of Xenograft Pancreatic Tumors. Ultrasound Med Biol 2017 43(12):2891–903 doi 10.1016/j.ultrasmedbio.2017.08.008. [PubMed: 28964615]
34. Samkoe KS, Chen A, Rizvi I, O'Hara JA, Hoopes PJ, Pereira SP, et al. Imaging tumor variation in response to photodynamic therapy in pancreatic cancer xenograft models. Int J Radiat Oncol Biol Phys 2010;76(1):251–9 doi 10.1016/j.ijrobp.2009.08.041. [PubMed: 20005458]
35. Chen B, Pogue BW, Zhou X, O'Hara JA, Solban N, Demidenko E, et al. Effect of tumor host microenvironment on photodynamic therapy in a rat prostate tumor model. Clin Cancer Res 2005;11(2 Pt 1):720–7. [PubMed: 15701861]
36. Chen B, Pogue BW, Goodwin IA, O'Hara JA, Wilmot CM, Hutchins JE, et al. Blood flow dynamics after photodynamic therapy with verteporfin in the RIF-1 tumor. Radiat Res 2003;160(4):452–9 doi 10.1667/RR3059. [PubMed: 12968929]
37. Jacobetz MA, Chan DS, Neesse A, Bapiro TE, Cook N, Frese KK, et al. Hyaluronan impairs vascular function and drug delivery in a mouse model of pancreatic cancer. Gut 2013;62(1):112–20 doi 10.1136/gutjnl-2012-302529. [PubMed: 22466618]
38. Hocker GB. Fiber-optic sensing of pressure and temperature. Appl Opt 1979;18(9):1445–8 doi 10.1364/AO.18.001445. [PubMed: 20212866]
39. Rahib L, Smith BD, Aizenberg R, Rosenzweig AB, Fleshman JM, Matrisian LM. Projecting Cancer Incidence and Deaths to 2030: The Unexpected Burden of Thyroid, Liver, and Pancreas Cancers in the United States (vol 74, pg 2913, 2014). Cancer research 2014;74(14):4006- doi 10.1158/0008-5472.Can-14-1642.
40. Gardian K, Janczewska S, Durlik M. Microenvironment elements involved in the development of pancreatic cancer tumor. Gastroenterol Res Pract 2012;2012:585674 doi 10.1155/2012/585674. [PubMed: 23304126]
41. Jain RK. Tumor microenvironment and microcirculation: Role in drug delivery. Ann Oncol 1998;9:24-.
42. Hingorani SR, Harris WP, Beck JT, Berdov BA, Wagner SA, Pshevlotsky EM, et al. Phase Ib Study of PEGylated Recombinant Human Hyaluronidase and Gemcitabine in Patients with Advanced Pancreatic Cancer. Clin Cancer Res 2016;22(12):2848–54 doi 10.1158/1078-0432.Ccr-15-2010. [PubMed: 26813359]
43. Hingorani SR, Thaddeus J, Berdov BA, Wagner SA, Pshevlotsky EM, Tjulandin SA, et al. A phase 1b study of gemcitabine plus PEGPH20 (pegylated recombinant human hyaluronidase) in patients with stage IV previously untreated pancreatic cancer. Eur J Cancer 2013;49:S619–S.
44. Riegler J, Labyed Y, Rosenzweig S, Javinal V, Castiglioni A, Dominguez CX, et al. Tumor Elastography and Its Association with Collagen and the Tumor Microenvironment. Clin Cancer Res 2018 doi 10.1158/1078-0432.ccr-17-3262.
45. Multhoff G, Vaupel P. Radiation-induced changes in microcirculation and interstitial fluid pressure affecting the delivery of macromolecules and nanotherapeutics to tumors. Front Oncol 2012;2:165 doi 10.3389/fonc.2012.00165. [PubMed: 23162794]

46. Yeo SG, Kim JS, Cho MJ, Kim KH, Kim JS. Interstitial Fluid Pressure as a Prognostic Factor in Cervical Cancer Following Radiation Therapy. Clin Cancer Res 2009;15(19):6201–7 doi 10.1158/1078-0432.Ccr-09-0560. [PubMed: 19773374]

47. Znati CA, Rosenstein M, Boucher Y, Epperly MW, Bloomer WD, Jain RK. Effect of radiation on interstitial fluid pressure and oxygenation in a human tumor xenograft. Cancer research 1996;56(5):964–68. [PubMed: 8640786]

48. Connolly KA, Belt BA, Figueroa NM, Murthy A, Patel A, Kim M, et al. Increasing the efficacy of radiotherapy by modulating the CCR2/CCR5 chemokine axes. Oncotarget 2016 doi 10.18632/oncotarget.13287.

Statement of translational relevance

Surgical resection has prolonged life of a small percentage of pancreatic cancer patients (< 20%). For a subset of patients with borderline resectable tumors, neoadjuvant therapy can work to downstage the tumor and enable surgical resection, but for many patients high tissue pressure prevents neoadjuvant chemotherapeutics from reaching the tumor interior. Although no imaging technique can measure tissue pressure, ultrasound elastography can measure shear modulus, an excellent surrogate for tissue pressure. Understanding the relationship between shear modulus and features of the tumor microenvironment (collagen density, hyaluronic acid content, and patent vessel density) known to impact tissue pressure and drug delivery would allow us to understand how well elastography can monitor changes in the tumor microenvironment of pancreatic patients undergoing systemic therapies.

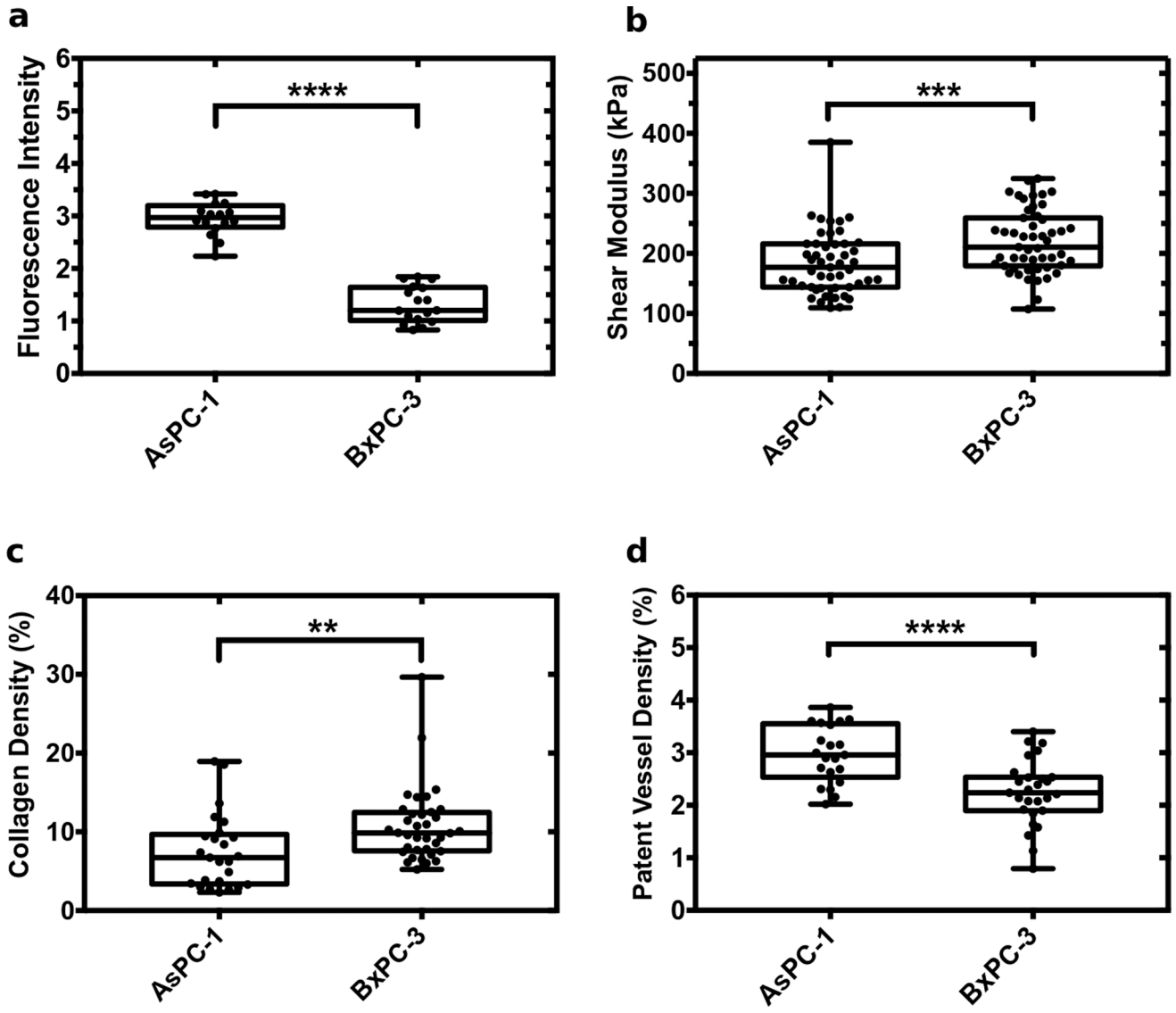

Figure 1:

Box plots of elasticity and histological markers measured for AsPC-1 and BxPC-3 tumors. Showing (a) fluorescence intensity of verteporfin, (b) mean shear modulus, (c) collagen density, and (d) patent vessel density. **** represents $p < 0.0001$, *** represents p values between 0.0001 to 0.001, and ** represents p values between 0.001 to 0.01.

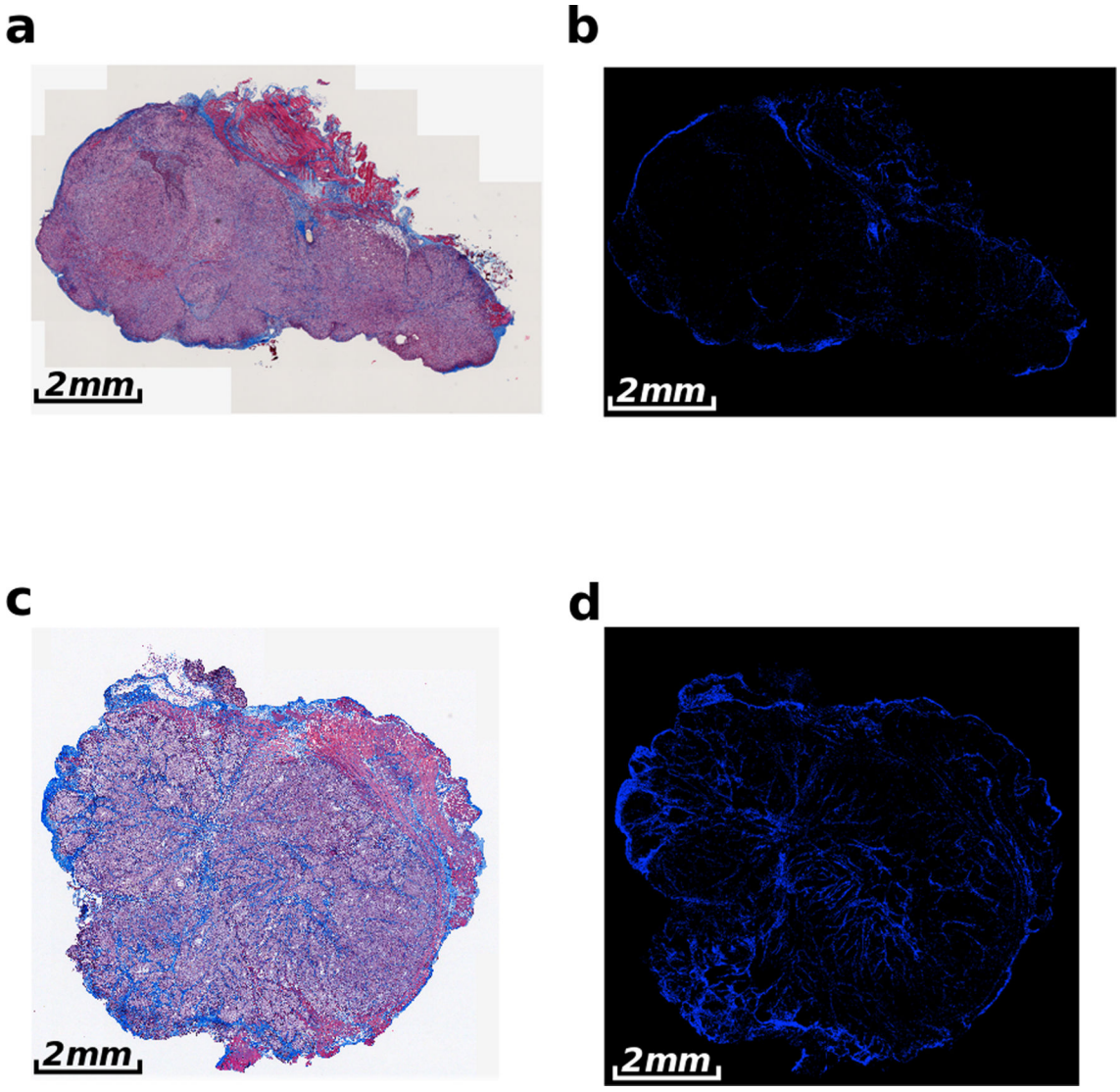

Figure 2:

Representative Masson's trichrome stained images of AsPC-1 and BxPC-3 tumors implanted into the pancreas of nude mice. Showing (a) AsPC-1 tumor and (b) color-segmented collagen distribution of the AsPC-1 tumor. (c) BxPC-3 tumor with (d) corresponding color-segmented collagen distribution. The AsPC-1 tumors in (a) and (b) have a collagen density of 5.6 ± 1.4%, in comparison to the collagen density of 12.5 ± 1.1% for the BxPC-3 tumor in (c) and (d).

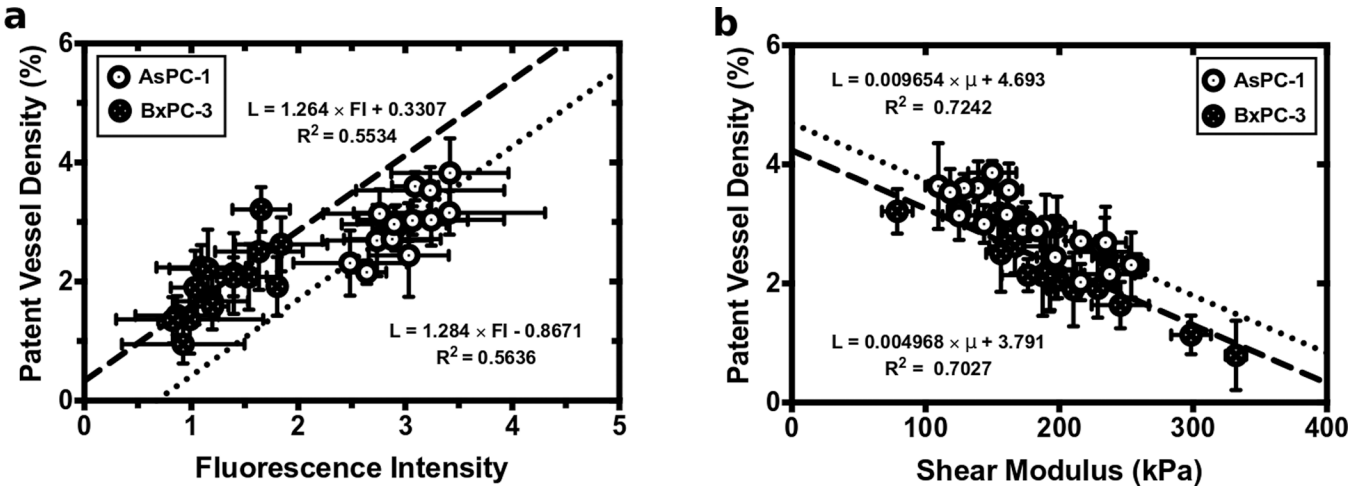

Figure 3:

Patent vessel density was compared to (a) calibrated fluorescence intensity and (b) shear modulus for both the AsPC-1 and BxPC-3 tumors.

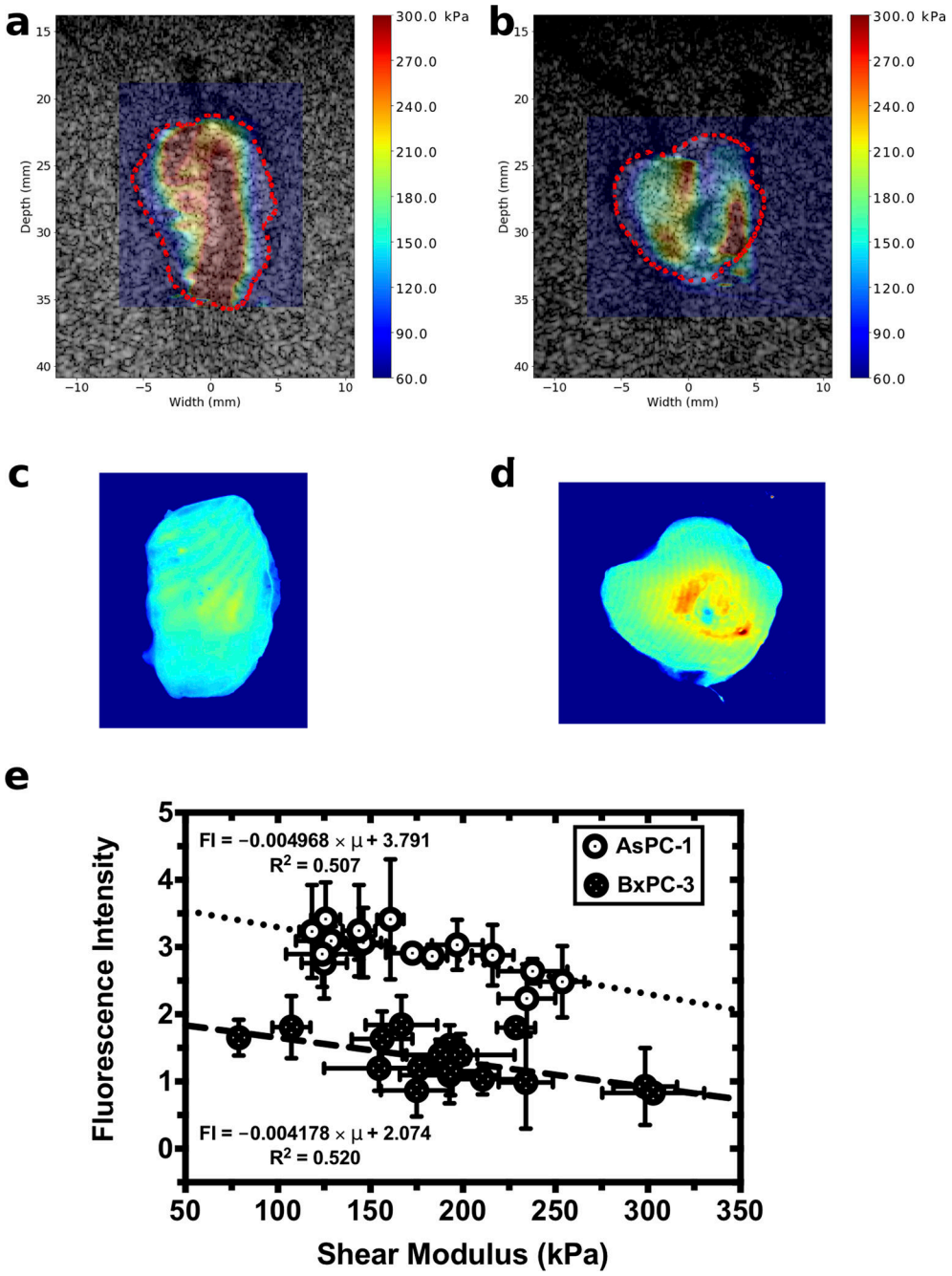

Figure 4:

Calibrated fluorescence intensity maps and elastographic imaging obtained from AsPC-1 and BxPC-3 tumors. Shear modulus overlaid on sonograms for a (a) AsPC-1 tumor and (b) BxPC-3 tumor. Calibrated fluorescence intensity maps obtained from the corresponding (c) AsPC-1 and (d) BxPC-3 tumors. (e) Fluorescence intensity plotted as a function of tumor shear modulus.

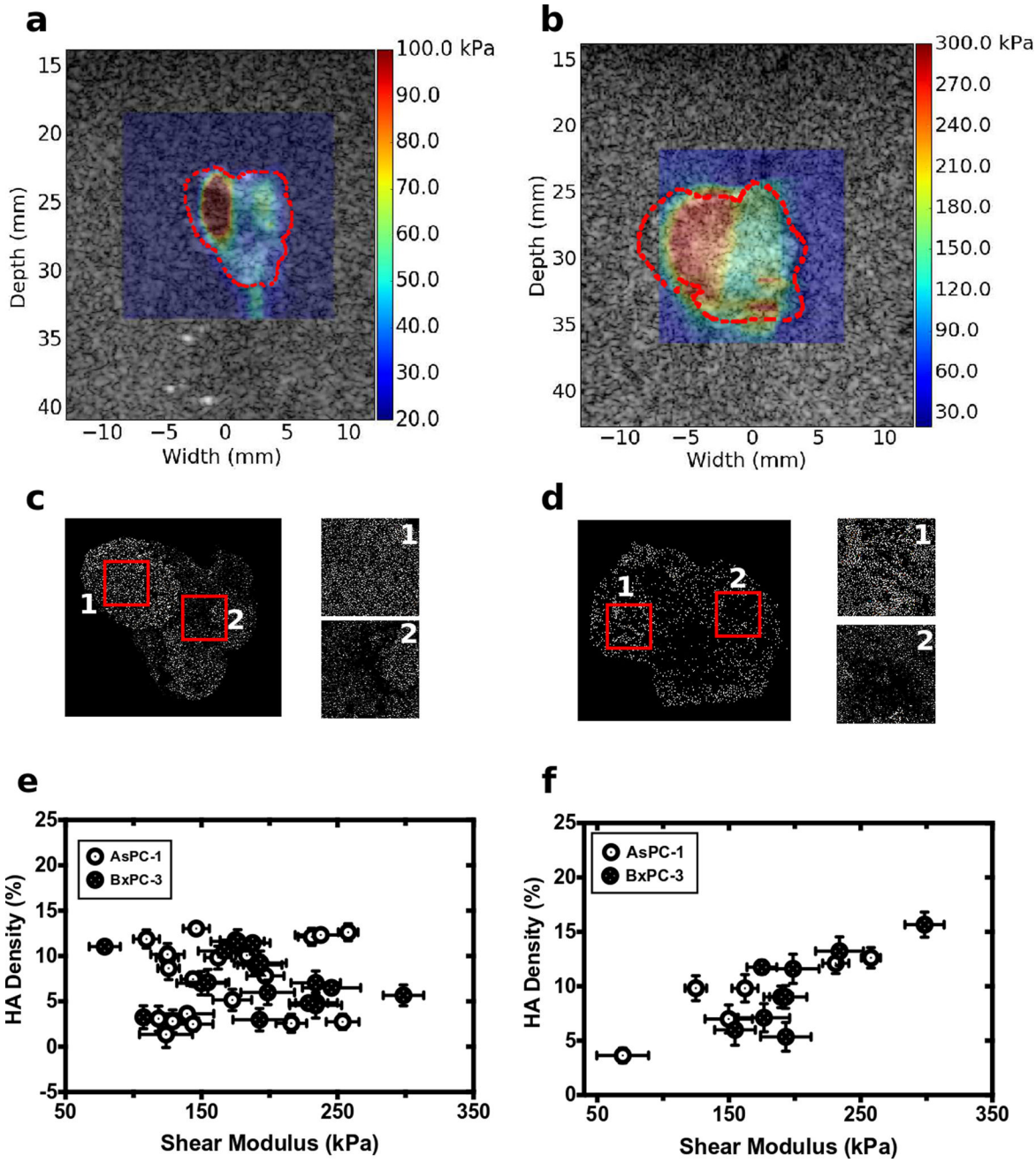

Figure 5:

Shear modulus overlaid on sonograms for the representative (a) AsPC-1 and (b) BxPC-3 tumors. (c) and (d) color-segmented hyaluronic acid distributions for the corresponding (c) AsPC-1 and (d) BxPC-3 tumors. Box #1 1 had an HA density of 15.6% with a shear modulus of 298.525 kPa; Box #2 had an HA density of 7.3% and shear modulus of 139 kPa. For the AsPC-1 tumor in (b) and (d), box #1 had an HA density of 9.8% with a shear modulus of 162 kPa; box #2 had an HA density of 3.6% and shear modulus of 69 kPa. (e) shows a scatter plot of global estimate of shear modulus and HA density calculated from

whole tumor slice. (f) show a local analysis of shear modulus and HA distribution shown in (c) and (d).